

Article

Detecting CdSe Nanomaterials with a Fluorescent Schiff Base Ligand

Jesús Sanmartín-Matalobos ^{1,*}, Pilar Bermejo-Barrera ², Ignacio Pérez-Juste ³, Matilde Fondo ¹, Ana M. García-Deibe ^{1,*} and Yeneva Alves-Iglesias ^{1,2}

¹ Coordination and Supramolecular Chemistry Group (SupraMetal), Department of Inorganic Chemistry, Faculty of Chemistry, Institute of Materials (iMATUS), Universidade de Santiago de Compostela, Avenida das Ciencias s/n, 15782 Santiago de Compostela, Spain

² Trace Element, Speciation and Spectroscopy Group (GETEE), Department of Analytical Chemistry, Nutrition and Bromatology, Faculty of Chemistry, Institute of Materials (iMATUS), Universidade de Santiago de Compostela, Avenida das Ciencias s/n, 15782 Santiago de Compostela, Spain

³ Departamento de Química Física, Facultad de Química, Edificio de Ciencias Experimentales, Universidade de Vigo, 36310 Vigo, Spain

* Correspondence: jesus.sanmartin@usc.es (J.S.-M.); ana.garcia.deibe@usc.es (A.M.G.-D.)

Abstract: We investigated the easily synthesized ligand H₃L as a fluorescent chemosensor for the detection of CdSe nanoparticles (CdSe NPs) and L-cysteine-capped CdSe quantum dots (CdSe-Cys QDs) in ethanol–water samples. A drastic quenching of the fluorescence emission of H₃L at 510 nm occurred, as a result of the addition of CdSe NPs and CdSe-Cys QDs. A solution of H₃L (1.26 ppb) showed sensitive responses to both CdSe NPs and CdSe-Cys QDs, with limits of detection (LOD) as low as 40 and 62 ppb, respectively. Moreover, using a smartphone color recognizer application, the fluorescence intensity response of H₃L-modified cellulose paper to CdSe-Cys QDs was recorded on a red channel (R), which allowed us to detect CdSe-Cys QDs with LOD = 15 ppb. Interference of some common metal nanomaterials (NMs), as well as metal ions, in the determination of CdSe NMs in solution was studied. The affinity of H₃L to CdSe NPs and CdSe-Cys QDs was spectroscopically determined. Scanning electron microscopy/energy-dispersive X-ray spectroscopy (SEM/EDX), micro-X-ray fluorescence (μ-XRF), ¹H-NMR, attenuated total reflection infrared spectroscopy (ATR-IR), and density functional theory (DFT) were also used to investigate the interaction of H₃L with CdSe NMs.

Keywords: CdSe; nanomaterials; quantum dots; Schiff base ligand; chemosensor; fluorescence



Citation: Sanmartín-Matalobos, J.; Bermejo-Barrera, P.; Pérez-Juste, I.; Fondo, M.; García-Deibe, A.M.; Alves-Iglesias, Y. Detecting CdSe Nanomaterials with a Fluorescent Schiff Base Ligand. *Chemosensors* **2022**, *10*, 394. <https://doi.org/10.3390/chemosensors10100394>

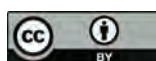
Academic Editor: Sofian Kanan

Received: 24 August 2022

Accepted: 25 September 2022

Published: 28 September 2022

Publisher's Note: MDPI stays neutral with regard to jurisdictional claims in published maps and institutional affiliations.



Copyright: © 2022 by the authors. Licensee MDPI, Basel, Switzerland. This article is an open access article distributed under the terms and conditions of the Creative Commons Attribution (CC BY) license (<https://creativecommons.org/licenses/by/4.0/>).

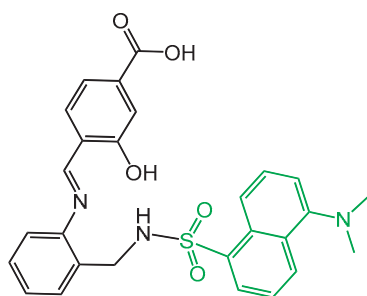
1. Introduction

Over the past few years, the unique chemical and biological properties of nanomaterials (NMs) has led to their ubiquitous presence in daily life. Amid the varied types of NMs, the II–VI semiconducting NMs have attracted much attention due to their outstanding electronic and optoelectronic properties [1–3]. In particular, one of the most widely used NMs of this type is cadmium selenide, as it has useful properties for biochemical sensors, biomedical imaging, photovoltaic applications, light-emitting diodes (LEDs), laser, thin-film transistors, or solar cells [3,4]. Another feature of this chalcogenide is its ability to form different nanostructures from simple nanoparticles to quantum dots (QDs), nanowires, nanobelts, or nanotubes, with dissimilar properties [4].

However, a clear negative consequence of this extensive use is the discharge into the environment of such noxious material. The toxicity of CdSe NMs results from the release of their harmful elements in an acidic environment. While cadmium is a well-known toxic element, which can induce oxidative stress, DNA damage, and apoptosis, excessive selenium can also induce toxicity [5–9], especially for aquatic life [10–13]. Therefore, the increasing concentrations of these NMs in the environment demands for reliable and affordable approaches for their detection.

Among the most suitable analytical methods useful for detecting NMs in aqueous samples, fluorescence-based sensing stands out. These methods involve simple solution assay processing, low cost, fast response, and high sensitivity, as well as high selectivity through molecular binding design. In this sense, some optical sensors have been developed for the detection of Ag NPs [14–16], but investigation of fluorescent sensors to detect CdSe NMs remains virtually unexplored [17].

Recently, we explored the chelating potential of two *N*-tosyl imines for CuO NPs sensing at neutral pH [18,19]. Here, we investigate the dansyl-based fluorescent probe H₃L (Scheme 1), which was easily synthesized by us [20], with the aim of detecting CdSe NMs in aqueous solution with short response time and sensing at basic pH.



Scheme 1. Schematic representation of H₃L, with the fluorophore highlighted in green.

H₃L displays an *N,N,O* donor set suitable to bind the Cd²⁺ ions present on the NM surface. In addition, both carboxylate and sulfonamide groups can contribute to the stabilization of the systems by interaction with the superficial ions of the NMs.

Herein, we are interested in studying the changes in the fluorescence emission spectra of H₃L upon increasing addition of CdSe NPs and CdSe-Cys QDs. Interference of some common NMs, as well as of metal ions, in the determination of CdSe NMs in ethanol/water samples was studied. Binding constants were also determined since these constants characterize the affinity of H₃L for NMs. Furthermore, interactions of H₃L with CdSe NPs and CdSe-Cys QDs were experimentally and theoretically (DFT calculations) investigated.

2. Materials and Methods

All starting materials and reagents, except H₃L and CdSe-Cys QDs, were commercially available and were used without further purification. The synthesis and characterization of H₃L were previously reported [20]. Fluorescence emission studies were performed on a Shimadzu RF-600 Spectro Fluorophotometer. Diffuse reflectance spectra were measured on a PerkinElmer LAMBDA 1050+ UV/Vis/NIR spectrophotometer equipped with an integrating sphere. Scanning electron microscopy (SEM) was applied to investigate the size and morphology, which was carried out under a ZEISS FESEM ULTRA, along with energy-dispersive X-ray (EDX) microanalysis. X-ray fluorescence was measured under vacuum (19.6 mbar) using a M4 TORNADO system (BRUKER), with an Rh tube, operating at 50 kV and 200 μ A. The fluorescence maps were collected for a total time of 2 ms per pixel, with a pixel size of 20 μ m. ¹H-NMR spectra (400 MHz) were measured in deuterated solvents using a Varian Inova 400 Spectrometer. *J* values are given in hertz. The infrared spectra were measured in the range 4000 to 400 cm⁻¹ wavenumber, using a Fourier-transform infrared (FTIR) spectrometer PerkinElmer Spectrum Two coupled with platinum diamond ATR, which consists of a diamond disc as an internal reflection element.

2.1. Sample Preparation

Samples for investigations on the interaction of H₃L with CdSe NMs were obtained by stirring an ethanol solution of H₃L at pH = 9 and a suspension of NMs in 2:1 molar ratio, at room temperature, for ca. 15 min. The sample was subsequently air-dried.

2.2. Computational Methods

Theoretical calculations on ligand–NMs models were performed employing density functional theory (DFT) methods, as implemented in Gaussian 09 [21]. Thus, M062X/6-31G* geometrical optimization of different starting structures of H₃L was performed. For H₃L, we tested that the M062X/6-31G* level provided results of comparable quality to those obtained with a more extended basis set as 6-311++G** (not included for brevity), but with a lower computational cost.

Models of various sizes have been used to evaluate the interaction of the ligand with CdSe NPs. The geometry for the smallest model, comprising one H₃L unit and a single CdSe unit, was optimized without restrictions. In the remaining cases, the geometries of the ligand over the surface were freely optimized, keeping a frozen structure for the metal selenide obtained from crystallographic data deposited with the Cambridge Structural Database (CSD).

Interaction energies, E_{int} , for these systems were evaluated as $E_{\text{int}} = E_{\text{complex}} - (E_{\text{H}_3\text{L}} + E_{\text{CdSe model}})$, where E_{complex} is the total energy of the ligand–NM interaction; $E_{\text{H}_3\text{L}}$ is the total energy of the monoanionic or dianionic form of the H₃L ligand, and $E_{\text{CdSe model}}$ is the energy of the different CdSe models indicated above. These interaction energies were evaluated by means of the natural energy decomposition analysis (NEDA) method included in the NBO7.0 program [22], such that the basis set superposition error was corrected by means of the counterpoise method.

2.3. Synthesis and Characterization of CdSe-Cys QDs

CdSe-Cys QDs were synthesized and characterized according to a method previously reported [23,24], which was slightly modified by us.

Firstly, 0.4 mmol (31.6 mg) of selenium and 1 mmol (38.6 mg) of sodium borohydride were dissolved in 10 mL of deionized water in a three-neck round-bottom flask, under argon atmosphere and constant stirring. The reduction of the selenium was kept in an ice bath for 2 h. In a second reaction flask, 0.4 mmol (123 mg) of cadmium nitrate tetrahydrate and 2 mmol (358 mg) of L-cysteine hydrochloride monohydrate were dissolved in 80 mL of deionized water. The pH of this solution was adjusted to 10 with a sodium hydroxide solution of 0.1 M. After this, the first solution was added to this second reaction flask, and the color of the resulting solution instantaneously changed from colorless to yellow. This solution was stirred and heated up to 100 °C. Monitoring of the QD size was performed every 10 min by both fluorescence emission [23] and UV/Vis absorption [25] spectrometry. After 1 h, the solution was red ($\lambda_{\text{abs}} = 451$ nm and $\lambda_{\text{em}} = 650$ nm, size of about 2.0 nm), and the reaction flask was subsequently kept in an ice bath to stop the reaction. Evaporation of the solution under reduced pressure led to one-fifth of its volume. Then, small portions of acetone were added to the solution, until it became cloudy, resulting in the precipitation of the CdSe-Cys QDs. The resulting supernatant was separated by centrifugation. Small portions of acetone were added again to this supernatant. This procedure was repeated three times. The precipitated QDs were dried at 40 °C, in an oven. Spectroscopy and microscopy characterizations are shown in Figures S1–S4.

Yield = 0.07 g. ¹H-NMR (400 MHz, D₂O, δ in ppm): 3.66 (t, 1H), 3.17 (dd, 1H), 2.96 (dd, 1H). ATR-IR (ν in cm⁻¹): $\nu(\text{HNH})$ 3222, $\nu_{\text{as}}(\text{COO}^-)$ 1557, $\nu_{\text{s}}(\text{COO}^-)$ 1393, $\nu(\text{CO})$ 1302. UV/Vis (water, λ in nm): 451. Fluorescence λ/nm : $\lambda_{\text{em}} = 632$ ($\lambda_{\text{ex}} = 400$, bandwidth of 15 nm).

2.4. Immobilization of H₃L onto Amine-Modified Cellulose Paper

For the immobilization of H₃L on cellulose paper (Whatman[®] qualitative filter paper, grade 2), we followed a previously reported method [26], which was slightly modified by us. Cellulose filter paper with a diameter of 55 mm was soaked in an ethanolic 3-aminopropyltrimethoxysilane solution (1 wt.%) for 1 h, at room temperature. The amine-modified cellulose paper was washed with copious ethanol, and dried under vacuum at 40 °C. *N*-Hydroxysuccinimide (NHS) and *N*-(3-dimethylaminopropyl)-*N*'-

ethylcarbodiimide hydrochloride (EDCHCl) were added in equimolar ratio (0.1 mmol) to a dimethylformamide solution (20 mL) of H₃L (0.1 mmol) to activate it. After stirring at room temperature for 3 h, triethylamine (0.3 mmol) was added to the reaction mixture, and the amine-modified cellulose paper was soaked in it overnight. Then, the immobilized H₃L onto amine-modified cellulose paper was washed with water and copious ethanol, and then dried under vacuum at 40 °C.

3. Results and Discussion

H₃L, in powder form, emits a yellow fluorescence under a UV light source at 365 nm (Figure 1, left bottom). An ethanol solution of H₃L at neutral pH emitted a maximal green fluorescence at about 510 nm, when it was exposed to visible light with a wavelength of 400 nm (Figure 1, at the bottom right). The use of polar solvents affords better emission and justified the use of ethanol to yield high green emission intensities, with Stokes shifts of about 110 nm. The study of the influence of pH on the fluorescence spectrum of H₃L (Figure 1, top) showed an increase in fluorescence intensity with increasing pH, which is consistent with the deprotonation of H₃L. Monodeprotonation of H₃L is expected at pH values below 7, since the pK_a value of the carboxylic group is around 4. Deprotonation of the phenol and sulfonamide groups requires higher pH values, since the pK_a of these groups is around 9. Moreover, pH values of about 6 (and lower ones) result in the protonation of the dimethylamino group, which is accompanied by a redshifted of λ_{em} to a wavelength of 520 nm (bathochromic shift). This can be due to the increase in the electron-withdrawing power of the sulfonyl group upon protonation of the amine nitrogen atom.

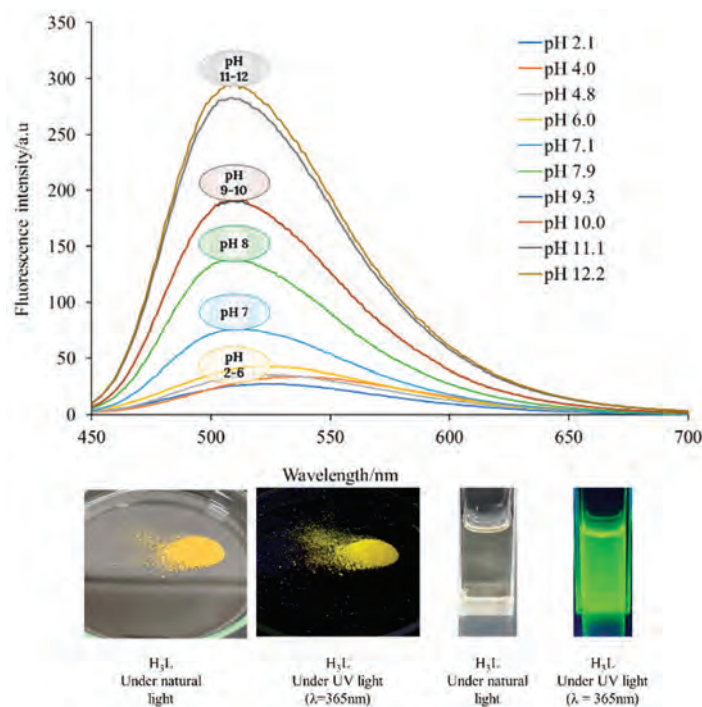


Figure 1. Top: Influence of pH on the fluorescence spectrum of H₃L (4.44×10^{-4} M) measured in ethanol (pH 2.1–12.2) at room temperature. Bottom: The effect of UV light (365 nm) on an ethanol solution (right) and a powdery sample (left) of H₃L.

3.1. Fluorescence Emission Studies on H₃L Solution upon Addition of CdSe NMs

The fluorescence intensity of an ethanol/water (80:20) solution of H₃L varied linearly with the concentrations of nonfluorescent CdSe NPs, as well as with weakly fluorescent CdSe-Cys QDs (λ_{em} = 632 nm), as shown in Figure S2 of the ESI.

In order to check the usefulness of H₃L as a chemosensor for the detection of CdSe nanomaterials at concentration ranges of ppm and ppb, we selected concentrations of H₃L

of 126 ppb and 1.26 ppb. With $[H_3L] = 126$ ppb, fluorescent emission varied linearly in the range 0–11.5 ppm of CdSe NPs and 0–10.5 ppm of CdSe-Cys QDs. The decrease by over 80% and 55% in the fluorescence emission of ethanol/water solutions (in 80:20 *v/v*) of H_3L ($\lambda_{em} = 540$ nm) upon addition of CdSe NPs ($\lambda_{em} = 536$ nm) and CdSe-Cys QDs ($\lambda_{em} = 536$ nm), respectively, are shown in Figure 2.

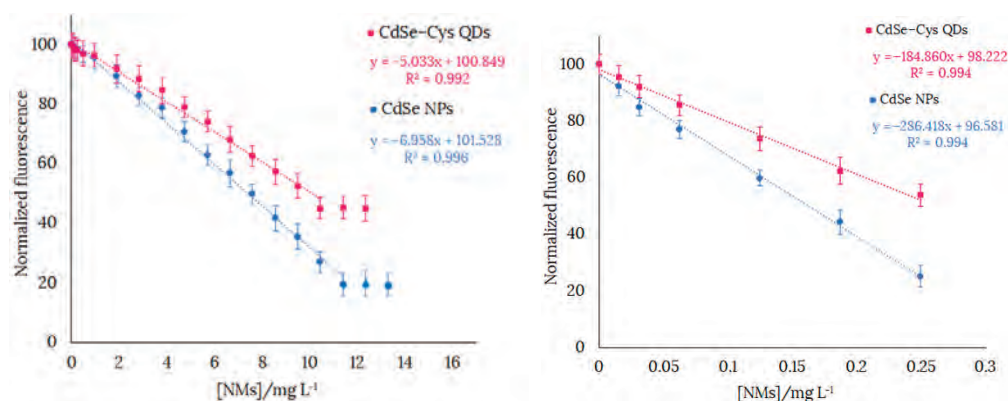


Figure 2. Calibration curve of fluorescence intensity of H_3L in 80:20 ethanol/water solution at pH 11 with gradual addition of NMs (until the fluorescence intensity stops decreasing). **Left:** $[H_3L] = 126$ ppb. **Right:** $[H_3L] = 1.26$ ppb. NaOH 0.1 M was used to deprotonate H_3L . Final volume of the solution = 4 mL. Each solution was sonicated for 1 min before being measured. $\lambda_{exc} = 400$ nm.

The limit of detection (LOD) and limit of quantification (LOQ) of H_3L are expressed as $LOD = 3SD/M$ and $LOQ = 10SD/M$, where SD is the standard deviation of the response, and M is the slope of the calibration curve [27]. LODs of CdSe NPs and CdSe-Cys QDs with $[H_3L] = 126$ ppb were 460 and 630 ppb, respectively. LOQs of CdSe NPs and CdSe-Cys with $[H_3L] = 126$ ppb were 1.52 and 2.11 ppm, respectively. LODs of CdSe NPs and CdSe-Cys QDs with $[H_3L] = 1.26$ ppb were 40 and 62 ppb, respectively. LOQs of CdSe NPs and CdSe-Cys with $[H_3L] = 1.26$ ppb were 134 and 207 ppb, respectively. The working range of H_3L was obtained using the LOQ as the minimum value that can be measured, with the highest value of $[NMs]$ at which linearity is still maintained as the maximum value. Therefore, the working ranges for detection of CdSe NPs and CdSe-Cys with $[H_3L] = 126$ ppb were 1.5–11.5 and 2.1–10.5 ppm, respectively.

3.2. Fluorescent Paper Detection of H_3L toward CdSe-Cys QDs

To facilitate detection of CdSe-Cys QDs, without the need to use a spectrofluorometer, we immobilized H_3L onto cellulose paper. The immobilization results in a slight color change of the paper, from white to pale yellow, which is visible with the naked eye. The ligand-modified cellulose paper upon soaking in CdSe-Cys QDs water solutions for 15 min exhibited a continuous color change from light green to bluish green under 365 nm ultraviolet light, when the CdSe-Cys QDs concentration increased from 5 to 100 ppb (Figure 3).

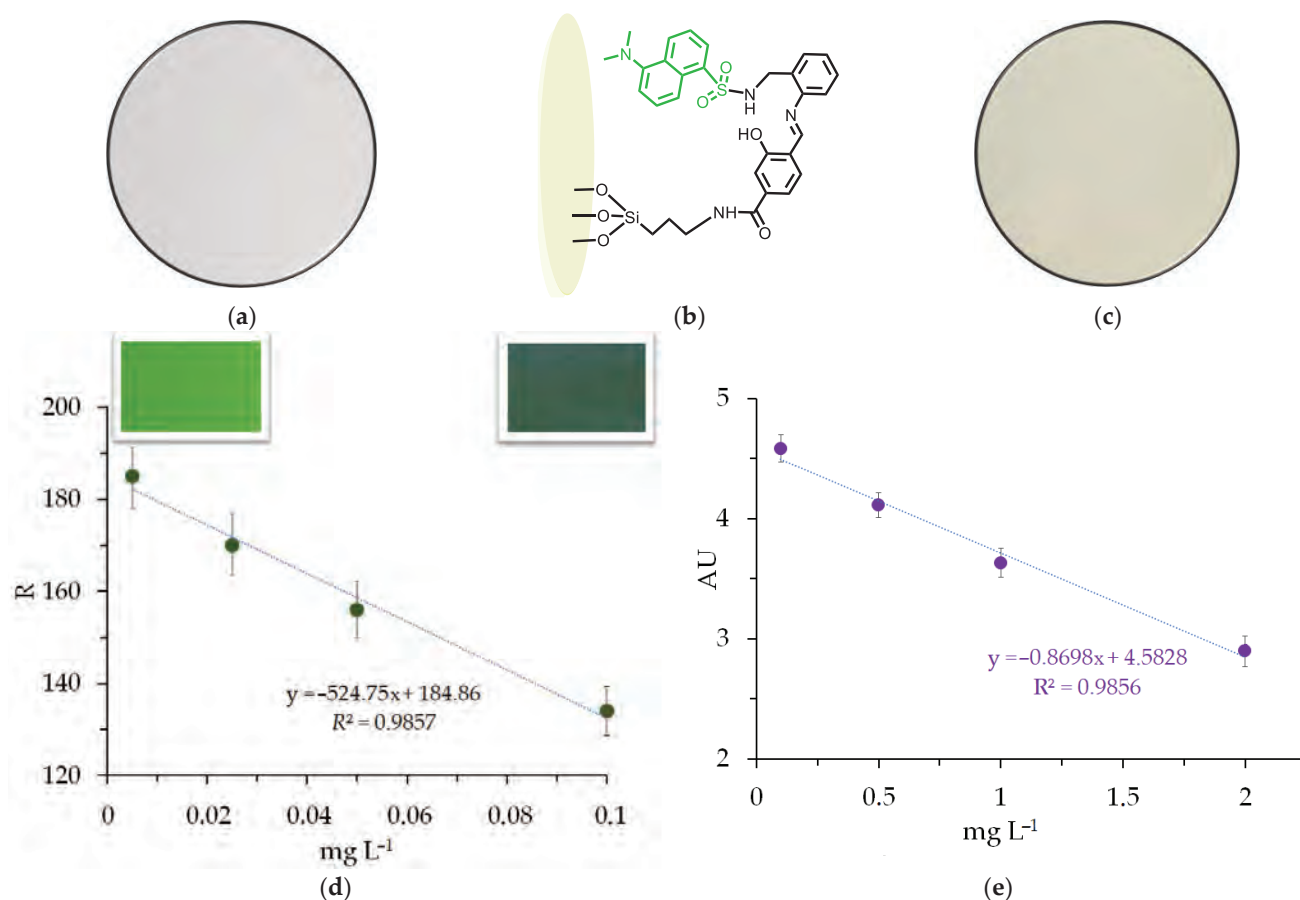


Figure 3. (a) Commercial cellulose paper under visible light. (b) Schematic representation of the ligand-modified cellulose paper. (c) Ligand-modified cellulose paper under visible light. (d) Variation of red coordinate in the RGB space of fluorescent images (excitation at 365 nm) of the ligand-modified cellulose paper upon soaking in CdSe-Cys QDs solution (5–100 ppb) for 15 min. Images (under UV light) of the fluorescent paper are included to show the color change. (e) Decrease in the absorbance of the band at 270 nm, with the increase in CdSe-Cys QDs concentration from 100 ppb to 2 ppm.

Since slight color changes cannot be easily observed with the naked eye, we digitized the color information (RGB value) of photographs corresponding to the paper under UV exciting radiation for analysis through the color recognizer application of a smartphone [28,29]. A series of photos were taken for three replicates of each assay with a smartphone under 365 nm ultraviolet light. The red–green–blue (RGB) values corresponding to these photos were obtained through the color recognizer application (RGB Color Detector) for further statistical analysis [30,31]. The RGB coordinates of five points on distinct parts of the paper for three replicates were obtained. Since the R coordinate shows sensitive response to CdSe-Cys QDs, the fluorescence intensity response, as an average of values for the measurements made, was recorded on the red channel. As Figure 3 shows, there was a good linear relationship between the red coordinate and the CdSe-Cys QDs concentration ($R^2 = 0.9857$). The LOD and LOQ calculation results were 15 and 50 ppb, respectively.

We also explored the use of UV/Vis/NIR spectrophotometry to discern the color change of the ligand-modified cellulose paper with the increase in the concentration of CdSe-Cys QDs. The ligand-modified cellulose paper upon soaking in CdSe-Cys QDs water solutions for 2 h exhibited a continuous decrease in the absorbance of each band of the diffuse reflectance spectrum, which showed three dominant signals located around 420, 330, and 270 nm. As the decrease in the absorbance was clearest in the band at 270 nm, we used this wavelength to study the response of the ligand-modified cellulose paper to the CdSe-Cys QDs concentration. Figure 3 (right) shows the linear decrease in the absorbance

of the band at 270 nm, when the CdSe-Cys QDs concentration increased from 100 ppb to 2 ppm. The LOD and LOQ calculation results were 245 and 815 ppb, respectively.

3.3. Affinity of H₃L to CdSe NMs

Since the reaction of H₃L with both CdSe NPs and CdSe-Cys QDs resulted in a decrease in its fluorescence emission, we investigated the quenching mechanism using Stern–Volmer plots ($F_0/F = 1 + K_{SV}[NMs]$). Figure 4 shows that the value of the quenching constant ($K_{SV} = \text{slope}$) decreased with increasing temperature, which is a sign of static quenching [32]. It must be noted that, for static quenching ($\tau_0/\tau = 1$), the K_{SV} value matched that of the binding constant (K_B) for the interaction under study. Thus, we found that the affinity of H₃L to the NMs studied at room temperature was as follows: CdSe NPs ($K_B = 4.42 \times 10^3 \text{ L}\cdot\text{mg}^{-1}$) > CdSe-Cys QDs ($K_B = 2.30 \times 10^3 \text{ L}\cdot\text{mg}^{-1}$). Values of Gibbs free energy (Table 1), which were determined from K_B , indicate that CdSe-H₃L NPs ($-20.46 \text{ kJ}\cdot\text{mg}^{-1}$) were more stable than CdSe-Cys-H₃L QDs ($-18.87 \text{ kJ}\cdot\text{mg}^{-1}$).

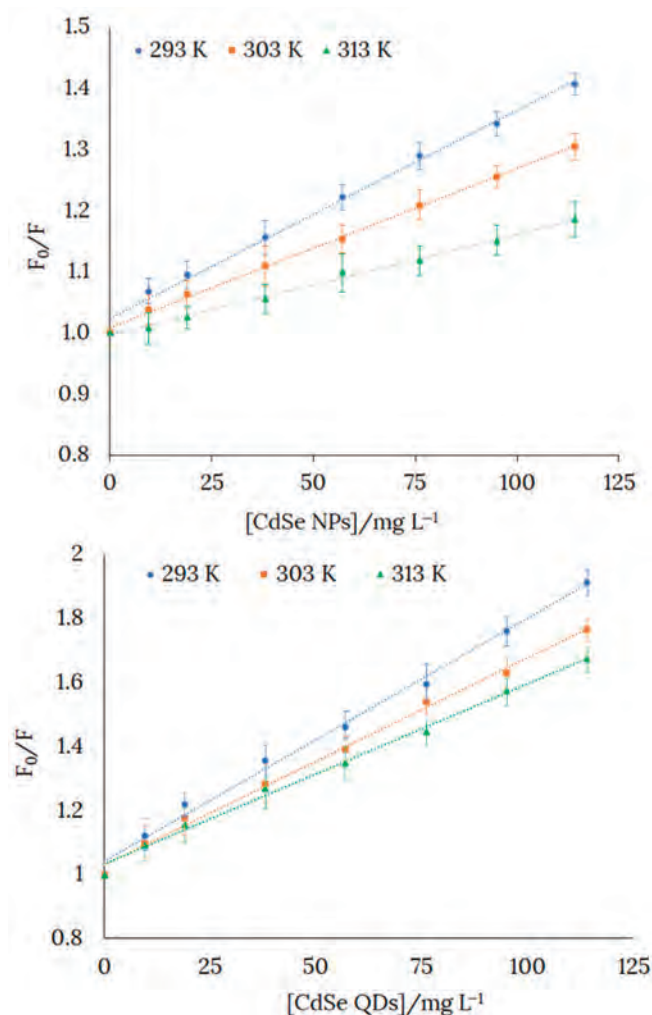


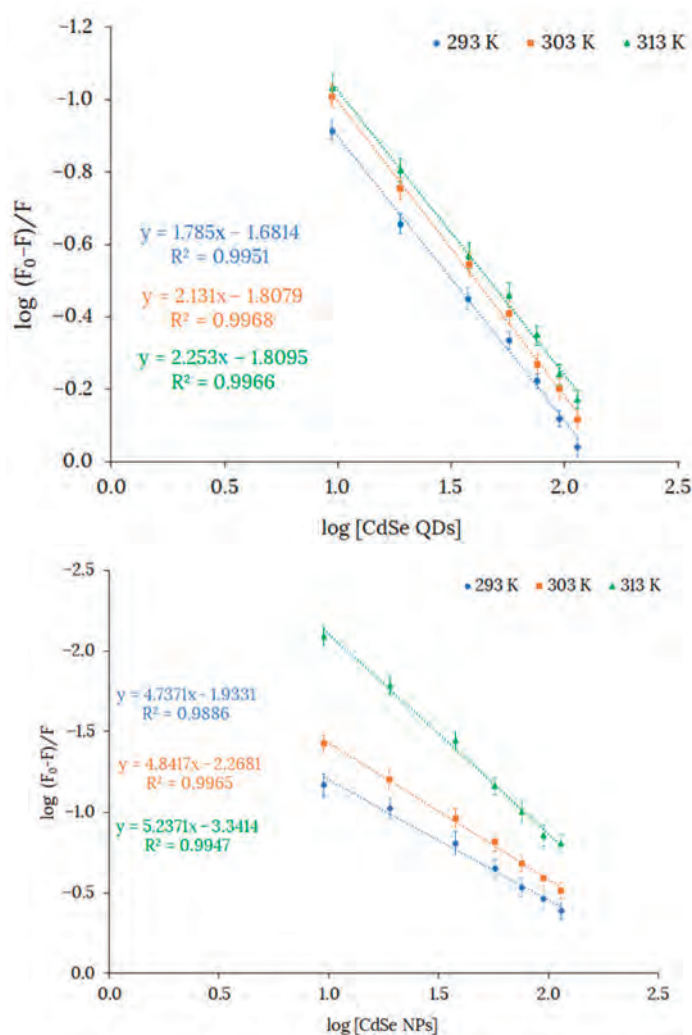
Figure 4. Plots of the intensities of the fluorescence spectra of H₃L (10^{-4} M) vs. the concentration of the quenchers CdSe NPs (**top**) and CdSe-Cys QDs (**bottom**) in an 80:20 ethanol/water solution. Slopes of the curves at 293, 303, and 313 K are Stern–Volmer constants K_{SV} ($K_{SV} = k_q\tau$, where τ is the lifetime of the fluorophore) at the cited temperatures.

Table 1. Values of Gibbs free energy and quenching constant for the reaction of H₃L with CdSe NPs and CdSe-Cys QDs.

Species	$\Delta G_{K_{sv}}^{293\text{ K}}$ $\text{kJ}\cdot\text{mol}^{-1}$ ($\text{kJ}\cdot\text{mg}^{-1}$)	$K_{sv}^{293\text{ K}} \text{ M}^{-1}$ ($\text{L}\cdot\text{mg}^{-1}$)	$K_{sv}^{303\text{ K}} \text{ M}^{-1}$ ($\text{L}\cdot\text{mg}^{-1}$)	$K_{sv}^{313\text{ K}} \text{ M}^{-1}$ ($\text{L}\cdot\text{mg}^{-1}$)
CdSe NPs	−20.08 (−20.46)	3790 (4420)	3150 (3600)	2610 (2750)
CdSe-Cys QDs	(−18.87)	(2300)	(1800)	(1230)

Considering the higher affinity of H₃L for CdSe NPs compared to CdSe-Cys QDs, we studied the number of binding sites for H₃L on the surfaces of both CdSe NPs and CdSe-Cys QDs. The number of interaction binding sites (n) was determined using the Scatchard equation (Equation (1)), where F_0 and F are the relative fluorescence of H₃L in the absence and presence of NMs, respectively, K_B is the binding constant, and $[Q]$ is the quencher concentration [33]. The Scatchard equation linear graph of H₃L and NMs is shown in Figure 5.

$$\log\left(\frac{F_0 - F}{F}\right) = \log K_B + n \log[Q] \quad (1)$$

**Figure 5.** The Scatchard plot for binding H₃L to CdSe NPs (**bottom**) and CdSe-Cys QDs (**top**) at 293, 303, and 313 K and pH 11.

The number of binding sites (n) was around five at 293 K, suggesting five binding sites for H₃L on the CdSe NP surface. However, the number of binding sites was about two for H₃L on the CdSe-Cys QD surface. This is not surprising considering that many of the surface cadmium ions interact with cysteine through the sulfur atom. The interaction ratio slightly increased for all the interactions with rising temperature, probably because temperature favors the reactivity of surface metal ions.

3.4. Selectivity

In view of the higher affinity of H₃L to CdSe NPs, we studied the selectivity of H₃L as a probe for the cited NPs. As a criterion for interference, a $\pm 10\%$ variation of the average fluorescence intensity at the respective concentration of CdSe NPs was used. The selectivity of H₃L as a probe for CdSe NPs was tested in the presence of some common NMs such as Cu NPs, CuO NPs, ZnO NPs, and TiO₂ NPs, as well as some common metal ions in water, such as the following hard acids: Na⁺, K⁺, Mg²⁺, Ca²⁺, Fe³⁺, and Al³⁺ (Figure 6).

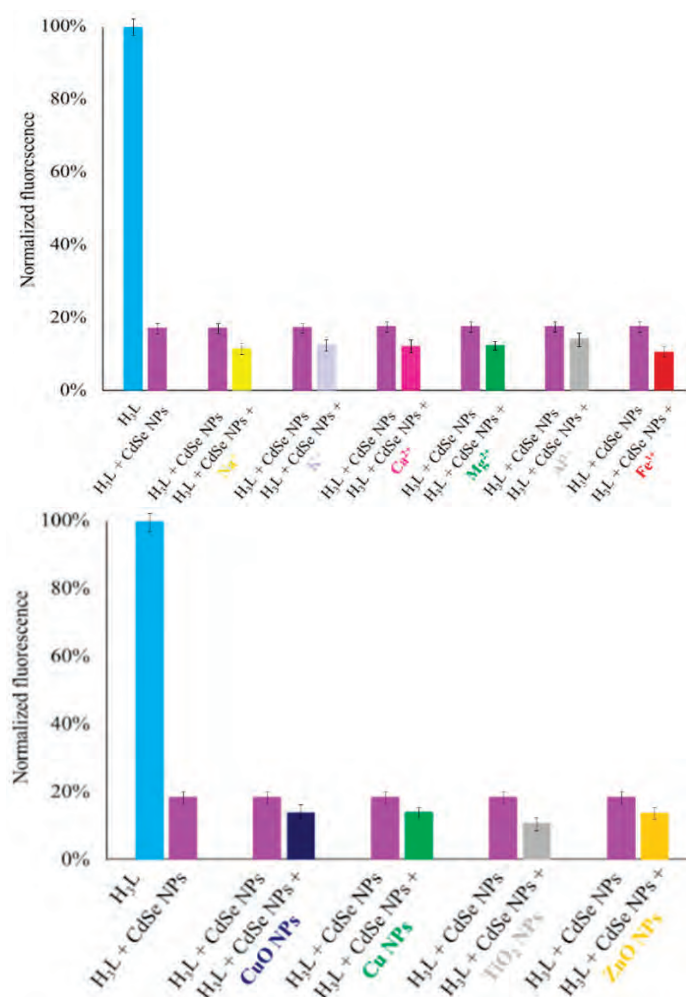


Figure 6. Fluorescence responses of H₃L (2.5 nM, 1.26 ppb) toward CdSe NPs (8 ppm) in the presence of various NPs (**bottom**) such as Cu NPs (8 ppm), CuO NPs (4 ppm), TiO₂ NPs (4 ppm), and ZnO NPs (4 ppm) and some common metal ions (**top**) such as Na⁺ (8 ppm), K⁺ (8 ppm), Fe³⁺ (8 ppm), Mg²⁺ (2 ppm), Ca²⁺ (2 ppm), and Al³⁺ (2 ppm). All experiments were performed in 4 mL of an ethanol–water solution in 80:20 *v/v* (pH 11) under $\lambda_{\text{exc}} = 400$ nm.

Results of three replicas of each assay showed that H₃L possessed selectivity toward CdSe NPs in the presence of Cu NPs, which could be tolerated in concentration of at least 8 ppm concentration, when the concentration of CdSe NPs was 8 ppm. Other common

NMs such as CuO NPs, ZnO NPs, and TiO₂ NPs could be tolerated in concentrations of at least 4 ppm without interference. Common metal ions in water such as Na⁺, K⁺, and Fe³⁺, in 8 ppm concentration, also did not interfere with the detection of CdSe NPs. Mg²⁺, Ca²⁺, and Al³⁺ ions could be tolerated in concentrations of at least 2 ppm without interference.

3.5. Investigations on the Interaction of H₃L with CdSe NMs

Scanning electron microscopy/energy-dispersive X-ray spectroscopy (SEM/EDX), micro-X-ray fluorescence (μ -XRF), nuclear magnetic resonance (¹H-NMR), total reflection infrared spectroscopy (ATR-IR), and density functional theory (DFT) were used to investigate the reaction products of CdSe NPs and CdSe-Cys QDs with H₃L.

3.5.1. Scanning Electron Microscopy/Energy-Dispersive X-ray Spectroscopy

The reaction products of CdSe NPs and CdSe-Cys QDs with H₃L were analyzed using SEM. As it can be seen in the SEM micrograph shown in Figure 7a, the reaction product of CdSe NPs with H₃L agglomerated to form clusters. These were made up of irregular nanocrystals with a size below 100 nm.

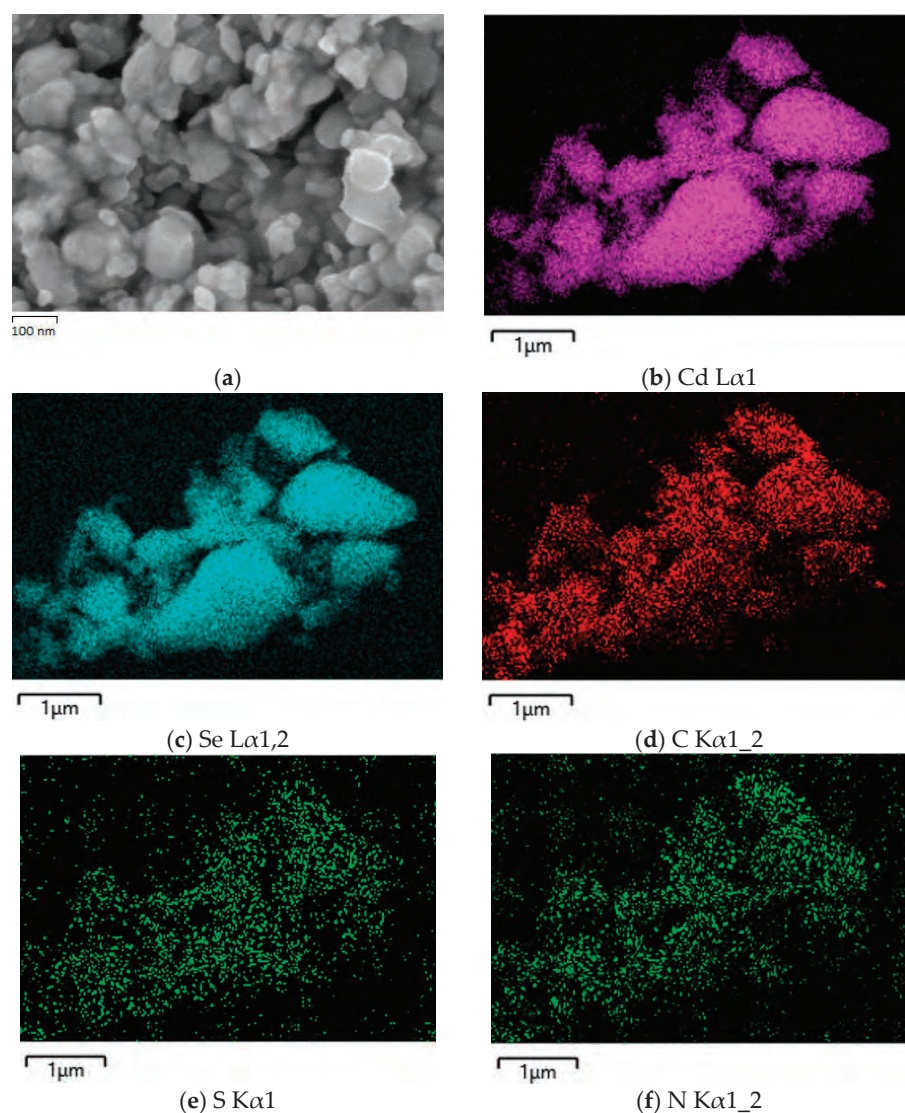


Figure 7. Cont.

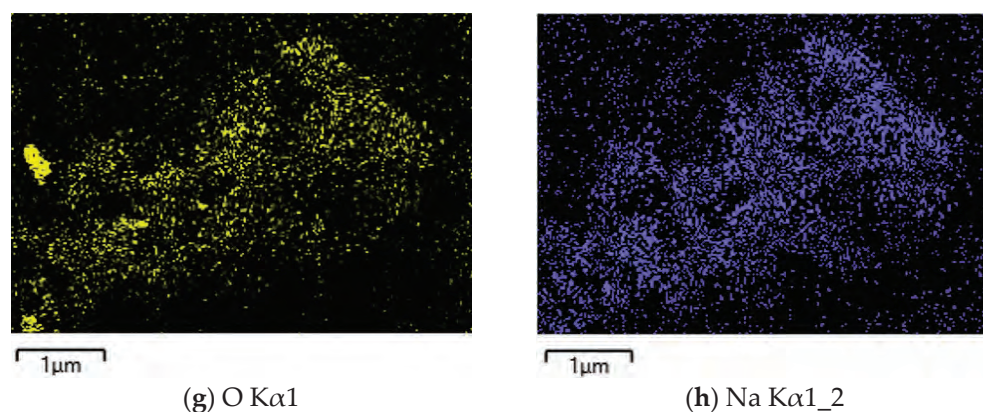


Figure 7. (a) SEM micrograph of the raw reaction product of CdSe NPs with H₃L (as carboxylate sodium salt). (b–h) EDX mapping pattern of different elements: Cd, Se, C, N, O, S, and Na.

A combination of SEM and EDX was used to generate a ‘map’ of element distributions in the raw sample. The EDX analysis showed the presence of Cd, Se, C, N, O, S, and Na elements with both uniform and similar spatial distribution patterns, supporting the existence of the interaction of H₃L (as carboxylate sodium salt) with CdSe NPs. Similarly, the EDX analysis of the reaction product of CdSe-Cys QDs with H₃L was in accordance with the formation of bonds between these species (Figure S5).

3.5.2. Micro-X-ray Fluorescence

Figure 8 shows the peaks corresponding to the characteristic X-ray fluorescence emission of the chemical elements in the reaction product of CdSe NPs with H₃L. The μ-XRF analysis indicates that the polycrystalline sample of the reaction product of CdSe NPs with H₃L (as carboxylate sodium salt) contained metal and sulfur in 53:1 ratio by weight, which was coherent with a 15:1 molar ratio (CdSe:H₃L) in the sample. μ-XRF mapping was used to probe the homogeneous distribution of cadmium and selenium within the sample, which supported the existence of bonding between CdSe NPs and H₃L.

3.5.3. ¹H Nuclear Magnetic Resonance

The ¹H-NMR spectrum of the reaction product of CdSe-Cys QDs with H₃L showed the expected proton signals, in accordance with the observations in the spectra of CdSe-Cys QDs and H₃L, as free species (Figures 9 and S6). The analysis of the region between 2.8 and 4.6 ppm clearly showed the characteristic signals of methyl and methylene protons of H₃L at 2.87 and 4.28 ppm, respectively, whereas the methanetriyl proton of L-Cys was observed at 4.52 ppm.

The interaction between CdSe-Cys QDs and H₃L did not result in significant shifts of their signals. The only noteworthy shift corresponded to the methanetriyl proton, which was shifted 0.05 ppm toward the low field. The overlapping of the methylene signal of L-Cys with the methyl proton of the deuterated solvent (methanol-*d*₄) prevented its observation at 3.31 ppm. On the basis of the corresponding integration values, it was possible to deduce that the cysteine:H₃L molar ratio was about 20:1 on the QD surface.

3.5.4. Attenuated Total Reflection Infrared Spectroscopy

The IR spectra of the reaction products of CdSe NPs and CdSe-Cys QDs with H₃L clearly show the absence of the band at about 3283 cm^{−1} attributable to ν OH/ν NH modes. This fact evidences the bideprotonation of the Schiff base ligand (Figures 10 and S7). Furthermore, the presence of a medium-intensity narrow band at about 1616 cm^{−1} is clear, which was attributable to the coordinate imino group of the ligand.

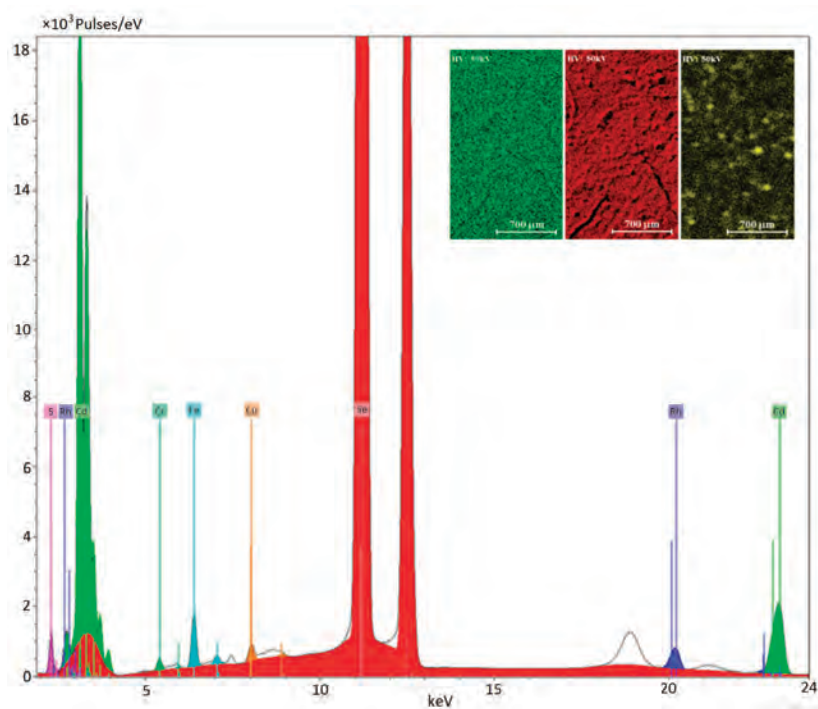


Figure 8. Bottom: XRF spectrum of the reaction product of CdSe NPs with H₃L. X-axis: energy (keV), Y-axis: intensity. **Top:** XRF mapping of the reaction product between CdSe NPs and H₃L with elemental distribution of sulfur (yellow), selenium (red), and cadmium (green) on the sample surface.

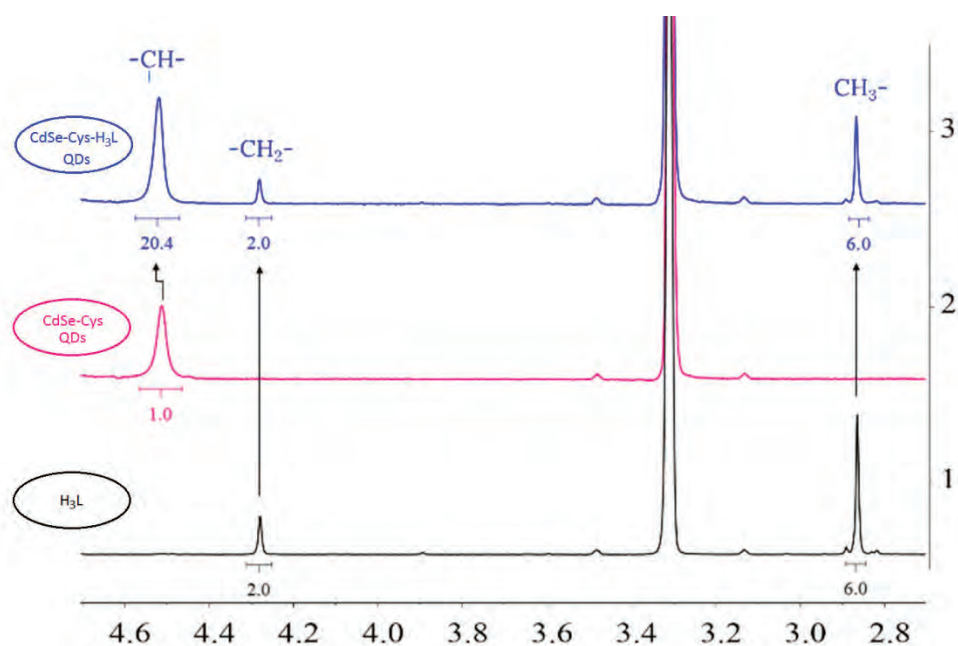


Figure 9. ¹H-NMR spectrum of the reaction product of CdSe-Cys QDs with H₃L (range: 4.8 to 2.6 ppm) in methanol-d₄. The spectra of CdSe-Cys QDs and H₃L, as free species, are included for comparison. Integration values are under the corresponding signals.

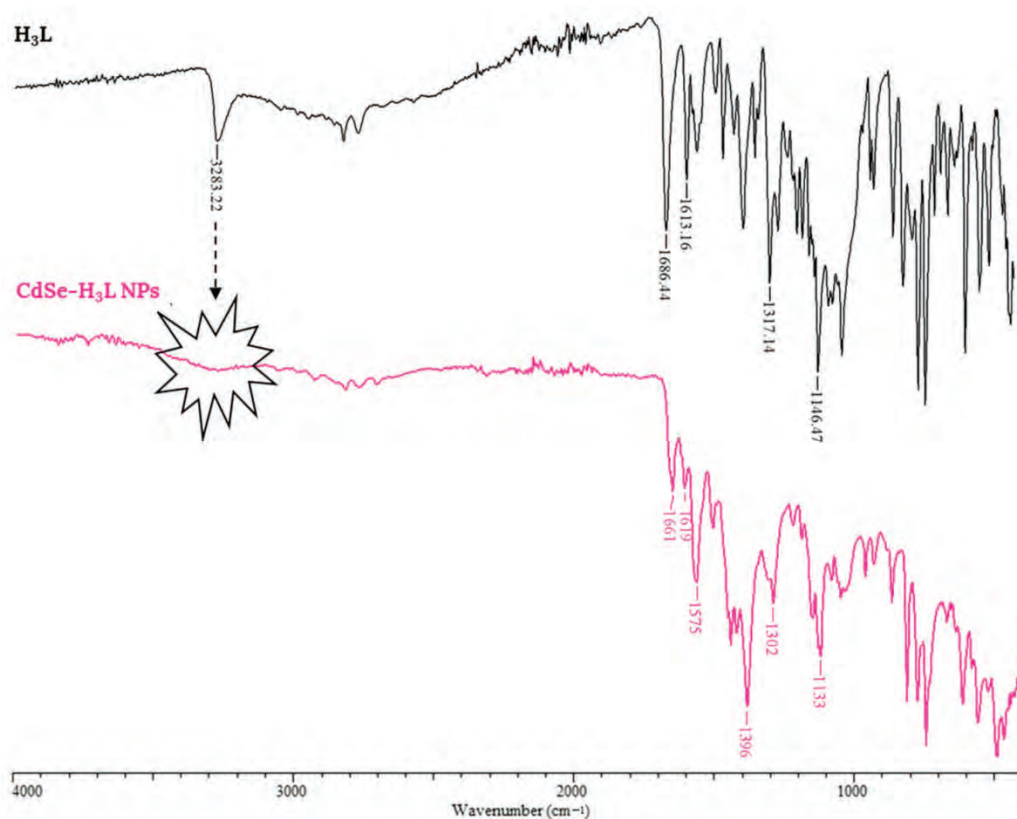


Figure 10. ATR-IR spectra of H₃L (top) and CdSe-H₃L NPs (bottom).

The bideprotonation and the shift of the narrow band of medium intensity seem to indicate that the interaction between H₃L and the NMs surface took place through the O_{phenol}, N_{imine}, and N_{sulfonamide} atoms of the ligand.

In addition, the observation of two bands attributable to $\nu_{as}(\text{COO}^-)$ and $\nu_s(\text{COO}^-)$ at about 1575 and 1396 cm⁻¹, respectively, was a clear sign of deprotonation of the carboxyl group in the ligand [34,35], coherent with the formation of the carboxylate sodium salt.

3.5.5. DFT Calculations

Several models of CdSe NPs were considered to mimic the interaction with H₃L using DFT calculations [19] (Table S1). The largest model studied comprised one unit of the ligand interacting with a sheet of 35 units of CdSe. This size was chosen to allow a complete interaction between H₃L and the CdSe surface. The geometry of this surface corresponds to the (0,0,1) facet from a crystal structure available from CSD, because it contains the maximum number of superficial cadmium atoms available to interact with the ligand. Particular attention was devoted to establishing the preference of a dianionic (as a phenolate and sulfonamide anion) or a monoanionic (as only phenolate) form of the ligand to interact with the metal ions on the CdSe NP surface. Figure 11 shows the DFT models obtained for the interaction of CdSe NPs with a dianionic ligand, as well as CdSe NPs with a monodeprotonated ligand.

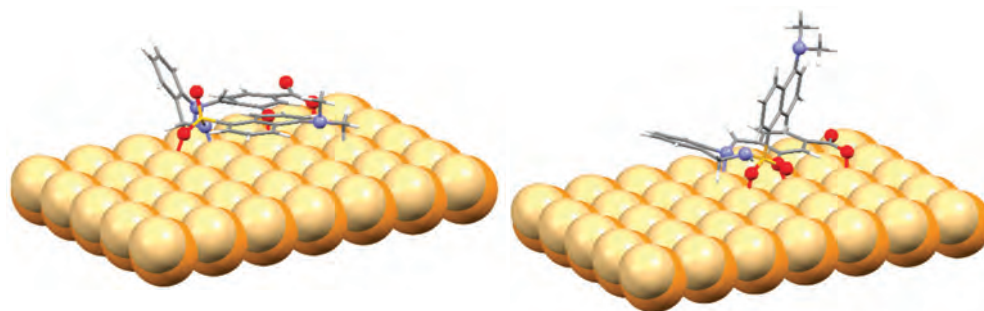


Figure 11. DFT models for the H₃L–NMs interaction.

For these models, interactions of the dianionic form of the ligand showed higher stabilization energies (−197.6 kcal/mol) than those of the monoanionic ones (−110.2 kcal/mol). The same trend was observed for all the diverse models considered, even with the smaller models employed here, which considered the interaction between the ligand and a single CdSe unit (Table S1). These theoretical results confirm that the interaction between H₃L and CdSe NPs surface took place through the O_{phenol}, N_{imine}, and N_{sulfonamide} atoms of the dianionic ligand (as phenolate and sulfonamide anion). In addition, the interactions of the surface metal ions with the oxygen atoms of the carboxylate and the sulfonamide groups could contribute to the stabilization of these systems.

The models also showed that the ligand changed its conformation, with respect to that of the isolated ligand, to maximize the interaction with the CdSe NP surface. Thus, a less folded ligand overlapped on the surface, giving rise to additional interactions, such as S=O⋯Cd, which also contributed to the stabilization of the interaction.

4. Conclusions

We probed that, at room temperature, CdSe NPs and CdSe–Cys QDs quickly interact with H₃L, especially at basic pH. The fluorescence intensity of H₃L in aqueous solution linearly decreased with increasing concentration of CdSe NMs. The working ranges for detection of CdSe NPs, and CdSe–Cys could be fine-tuned by varying the concentration of H₃L. A solution of H₃L (1.26 ppb) showed sensitive responses to CdSe NPs and CdSe–Cys QDs, with detection limits as low as 40 and 62 ppb, respectively. The limits of detection of CdSe NPs and CdSe–Cys QDs with [H₃L] = 126 ppb were 460 and 630 ppb, respectively. Moreover, using a smartphone color recognizer application, the fluorescence intensity response of H₃L-modified cellulose paper to CdSe–Cys QDs was recorded in the red channel (R), which allowed us to detect CdSe–Cys QDs with LOD = 15 ppb. Diffuse reflectance spectrophotometry also allowed detecting CdSe–Cys QDs using H₃L-modified cellulose paper (LOD = 245 ppb and LOQ = 815 ppb). H₃L possessed selectivity toward CdSe NPs in the presence of Cu NPs, which could be tolerated in concentration of at least 8 ppm concentration, when the concentration of CdSe NPs was 8 ppm. Other common NMs such as CuO NPs, ZnO NPs, and TiO₂ NPs could be tolerated in concentrations of at least 4 ppm without interference. Common metal ions in water such as Na⁺, K⁺, and Fe³⁺, in 8 ppm concentration, did not interfere with the detection of CdSe NPs. Mg²⁺, Ca²⁺, and Al³⁺ ions could be tolerated in concentrations of 2 ppm without interference.

We found that the affinity of H₃L to the NMs studied was as follows: CdSe NPs > CdSe–Cys QDs, and that H₃L used five binding sites on the surface of CdSe NPs, whereas it used only two binding sites on the CdSe–Cys QD surface. Moreover, we determined a 15:1 molar ratio (CdSe:H₃L) in the reaction product of CdSe NPs with H₃L, and a cysteine:H₃L molar ratio of about 20:1 on the CdSe–Cys QD surface. Lastly, theoretical results support that the interaction between H₃L and CdSe NPs took place through the O_{phenol}, N_{imine}, and N_{sulfonamide} atoms of the dianionic ligand (as a phenolate and sulfonamide anion), and that O atoms of the carboxylate and the sulfonamide groups contributed to the stabilization of the systems.

Supplementary Materials: The following supporting information can be downloaded at <https://www.mdpi.com/article/10.3390/chemosensors10100394/s1>: Figure S1: ^1H NMR spectrum of cysteine-capped CdSe QDs; Figure S2: UV-Vis spectrum of CdSe-Cys QDs; Figure S3: ATR-FTIR spectrum of CdSe-Cys QDs; Figure S4: SEM-EDX images of CdSe-Cys QDs; Figure S5: XRF spectrum and mapping of CdSe- H_3L NPs; Figure S6: ^1H NMR spectrum of CdSe-Cys- H_3L QDs; Figure S7: ATR-IR spectra of CdSe-Cys- H_3L QDs; Table S1: DFT models for the interaction H_3L -NMs.

Author Contributions: Conceptualization, J.S.-M. and P.B.-B.; methodology, Y.A.-I. and I.P.-J.; software, I.P.-J. and Y.A.-I.; validation, J.S.-M., I.P.-J. and P.B.-B.; formal analysis, I.P.-J., M.F. and Y.A.-I.; investigation, I.P.-J. and Y.A.-I.; resources, J.S.-M. and P.B.-B.; data curation, I.P.-J. and M.F.; writing—original draft preparation, J.S.-M. and Y.A.-I.; writing—review and editing, A.M.G.-D.; visualization, M.F.; supervision, J.S.-M.; project administration, P.B.-B.; funding acquisition, P.B.-B. All authors have read and agreed to the published version of the manuscript.

Funding: This research was funded by the Ministerio de Ciencia, Innovación y Universidades (RTI2018-099222-B-I00) and Interreg Atlantic Area, Poctep (ACUINANO Project).

Institutional Review Board Statement: Not applicable.

Informed Consent Statement: Not applicable.

Data Availability Statement: Not applicable.

Acknowledgments: We would like to thank the “Area de Infraestructuras de Investigación da USC” for the support provided for this work.

Conflicts of Interest: The authors declare no conflict of interest.

References

1. Divya; Kaur, G.; Asha, K.; Dass, S.; Shrivastav, R. Photoelectrochemical performance of Yb Co-doped $\text{BiV}_{0.98}\text{Mo}_{0.02}\text{O}_4$ thin films for Photoelectrochemical water splitting. *Mater. Today Proc.* **2022**, *49*, 738–743. [[CrossRef](#)]
2. Yu, Z.; Gong, H.; Xu, J.; Li, Y.; Zeng, Y.; Liu, X.; Tang, D. Exploiting Photoelectric Activities and Piezoelectric Properties of NaNbO_3 Semiconductors for Point-of-Care Immunoassay. *Anal. Chem.* **2022**, *94*, 3418–3426. [[CrossRef](#)] [[PubMed](#)]
3. Chopade, P.; Jagtap, S.; Gosavi, S. Material properties and potential applications of CdSe semiconductor nanocrystals. In *Nanoscale Compound Semiconductors and Their Optoelectronics Applications*; Pawade, V.B., Dhoble, S.J., Swart, H.C., Eds.; Woodhead Publishing: Cambridge, MA, USA, 2022; pp. 105–153. [[CrossRef](#)]
4. Jin, W.; Hu, L. Review on quasi one-dimensional CdSe nanomaterials: Synthesis and application in photodetectors. *Nanomaterials* **2019**, *9*, 1359. [[CrossRef](#)] [[PubMed](#)]
5. Derfus, A.M.; Chan, W.C.W.; Bhatia, S.N. Probing the Cytotoxicity of Semiconductor Quantum Dots. *Nano Lett.* **2004**, *4*, 11–18. [[CrossRef](#)]
6. Mahendra, S.; Zhu, H.; Colvin, V.L.; Alvarez, P.J. Quantum dot weathering results in microbial toxicity. *Environ. Sci. Technol.* **2008**, *42*, 9424–9430. [[CrossRef](#)]
7. Allocca, M.; Mattered, L.; Bauduin, A.; Miedziak, B.; Moros, M.; De Trizio, L.; Tino, A.; Reiss, P.; Ambrosone, A.; Tortiglione, C. An Integrated Multilevel Analysis Profiling Biosafety and Toxicity Induced by Indium- and Cadmium-Based Quantum Dots in Vivo. *Environ. Sci. Technol.* **2019**, *53*, 3938–3947. [[CrossRef](#)]
8. Su, Y.; Hu, M.; Fan, C.; He, Y.; Li, Q.; Li, W.; Wang, L.-H.; Shen, P.; Huang, Q. The cytotoxicity of CdTe quantum dots and the relative contributions from released cadmium ions and nanoparticle properties. *Biomaterials* **2010**, *31*, 4829–4834. [[CrossRef](#)]
9. Hu, L.; Zhong, H.; He, Z. The cytotoxicities in prokaryote and eukaryote varied for CdSe and CdSe/ZnS quantum dots and differed from cadmium ions. *Ecotoxicol. Environ. Saf.* **2019**, *181*, 336–344. [[CrossRef](#)]
10. Tarrahi, R.; Movafeghi, A.; Khataee, A.; Rezanejad, F.; Gohari, G. Evaluating the Toxic Impacts of Cadmium Selenide Nanoparticles on the Aquatic Plant. *Lemna minor*. *Molecules* **2019**, *24*, 410. [[CrossRef](#)]
11. Zhang, W.; Lin, K.; Sun, X.; Dong, Q.; Huang, C.; Wang, H.; Guo, M.; Cui, X. Toxicological effect of MPA-CdSe QDs exposure on zebrafish embryo and larvae. *Chemosphere* **2012**, *89*, 52–59. [[CrossRef](#)]
12. Morelli, V.; Cioni, P.; Posarelli, M.; Gabellieri, E. Chemical stability of CdSe quantum dots in seawater and their effects on a marine microalga. *Aquat. Toxicol.* **2012**, *122–123*, 153–162. [[CrossRef](#)] [[PubMed](#)]
13. Ambrosone, A.; Roopin, M.; Pelaz, B.; Abdelmonem, A.M.; Ackermann, L.-M.; Mattered, L.; Allocca, M.; Tino, A.; Klapper, M.; Parak, W.J.; et al. Dissecting common and divergent molecular pathways elicited by CdSe/ZnS quantum dots in freshwater and marine sentinel invertebrates. *Nanotoxicology* **2017**, *11*, 289–303. [[CrossRef](#)]
14. Chatterjee, A.; Santra, M.; Won, N.; Kim, V.; Kim, J.K.; Kim, S.B.; Ahn, K.H. Selective Fluorogenic and Chromogenic Probe for Detection of Silver Ions and Silver Nanoparticles in Aqueous Media. *J. Am. Chem. Soc.* **2009**, *131*, 2040–2041. [[CrossRef](#)]
15. Cayuela, A.; Soriano, M.L.; Valcárcel, M. Reusable sensor based on functionalized carbon dots for the detection of silver nanoparticles in cosmetics via inner filter effect. *Anal. Chim. Acta* **2015**, *872*, 70–76. [[CrossRef](#)] [[PubMed](#)]

16. Raz, S.R.; Leontaridou, M.; Bremer, M.G.E.G.; Peters, R.; Weigel, S. Development of surface plasmon resonance-based sensor for detection of silver nanoparticles in food and the environment. *Anal. Bioanal. Chem.* **2012**, *403*, 2843–2850. [[CrossRef](#)]
17. Sanmartín-Matalobos, J.; Bermejo-Barrera, P.; Aboal-Somoza, M.; Fondo, M.; García-Deibe, A.M.; Corredoira-Vázquez, J.; Alves-Iglesias, Y. Semiconductor Quantum Dots as Target Analytes: Properties, Surface Chemistry and Detection. *Nanomaterials* **2022**, *12*, 2501. [[CrossRef](#)] [[PubMed](#)]
18. Sanmartín-Matalobos, J.; García-Deibe, A.M.; Fondo, M.; Zarepour-Jevinani, M.; Domínguez-González, M.R.; Bermejo-Barrera, P. Exploration of an easily synthesized fluorescent probe for detecting copper in aqueous samples. *Dalton Trans.* **2017**, *46*, 15827–15835. [[CrossRef](#)]
19. Sanmartín-Matalobos, J.; García-Deibe, A.M.; Zarepour-Jevinani, M.; Aboal-Somoza, M.; Bermejo-Barrera, P.; Fondo, M. Exploring the Chelating Potential of an Easily Synthesized Schiff Base for Copper Sensing. *Crystals* **2020**, *10*, 235. [[CrossRef](#)]
20. Sanmartín-Matalobos, J.; Bermejo-Barrera, P.; Alves-Iglesias, Y.; García-Deibe, A.M.; Fondo, M. Synthesis and Characterization of a Dansyl-Based Fluorescent Probe for Analytical Purposes. *Chem. Proc.* **2022**, *8*, 76. [[CrossRef](#)]
21. Frisch, M.J.; Trucks, G.W.; Schlegel, H.B.; Scuseria, G.E.; Robb, M.A.; Cheeseman, J.R.; Scalmani, G.; Barone, V.; Petersson, G.A.; Nakatsuji, H.; et al. (Eds.) *Gaussian 09, Revision A.02*; Gaussian Inc.: Wallingford, CT, USA, 2016.
22. Glendinging, E.D.; Badenhop, J.K.; Reed, A.E.; Carpenter, J.E.; Bohmann, J.A.; Morales, C.M.; Karafiloglou, P.; Landis, C.R.; Weinhold, F. (Eds.) *NBO 7.0*; Theoretical Chemistry Institute, University of Wisconsin: Madison, WI, USA, 2018.
23. Santos, C.I.L.; Souza-Carvalho, M.; Raphael, E.; Dantas, C.; Ferrari, J.L.; Schiavon, M.A. Synthesis, Optical Characterization, and Size Distribution Determination by Curve Resolution Methods of Water-Soluble CdSe Quantum Dots. *Mater. Res.* **2016**, *19*, 1407–1416. [[CrossRef](#)]
24. Liu, P.; Wang, Q.; Li, X. Studies on CdSe/L-cysteine Quantum Dots Synthesized in Aqueous Solution for Biological Labeling. *J. Phys. Chem. C* **2009**, *113*, 7670–7676. [[CrossRef](#)]
25. Yu, W.W.; Qu, L.; Guo, W.; Peng, X. Experimental Determination of the Extinction Coefficient of CdTe, CdSe, and CdS Nanocrystals. *Chem. Mater.* **2003**, *15*, 2854–2860. [[CrossRef](#)]
26. Jeon, C.H.; Park, C.S.; Lee, C.S.; Ha, T.H. Simple immobilization of mercury ion chemosensors to solid substrate. *J. Ind. Eng. Chem.* **2018**, *57*, 370–376. [[CrossRef](#)]
27. Shrivastava, A.; Gupta, V. Methods for the determination of limit of detection and limit of quantitation of the analytical methods. *Chron. Young Sci.* **2011**, *2*, 1. [[CrossRef](#)]
28. Yang, F.; Lin, D.; Pan, L.; Zhu, J.; Shen, J.; Yang, L.; Jiang, C. Portable Smartphone Platform Based on a Single Dual-Emissive Ratiometric Fluorescent Probe for Visual Detection of Isopropanol in Exhaled Breath. *Anal. Chem.* **2021**, *93*, 14506–14513. [[CrossRef](#)]
29. Yan, F.; Hu, S.; Wang, Y.; Song, X.; Cao, C.; Wang, K.; Jing, C.; Zhang, G.; Liu, W. A multifunctional fluorescent probe for visualizing H₂S in wastewater with portable smartphone via fluorescent paper strip and sensing GSH in vivo. *J. Hazard. Mater.* **2021**, *406*, 124523. [[CrossRef](#)]
30. Verdugo-Naranjo, I.; Hamamura, A.C.; Arruda, G.V.; Cardoso, G.C.; Pavoni, J.F. Radiodermatitis grade estimation by RGB color imaging. *Artif. Life Robot.* **2022**, *27*, 58–63. [[CrossRef](#)]
31. Brachmann, E.; Rother, C. Visual Camera Re-Localization From RGB and RGB-D Images Using DSAC. *IEEE Trans. Pattern Anal. Mach. Intell.* **2022**, *44*, 5847–5865. [[CrossRef](#)]
32. Lakowicz, J.R. *Principles of Fluorescence Spectroscopy*, 3rd ed.; Springer Nature: Boston, MA, USA, 2006.
33. Moeno, S.; Nyokong, T. Opposing responses elicited by positively charged phthalocyanines in the presence of CdTe quantum dots. *J. Photochem. Photobiol. A* **2009**, *201*, 228–236. [[CrossRef](#)]
34. Oluwafemi, S.O.; Revaprasadu, N.; Ramirez, A.J. A novel one-pot route for the synthesis of water-soluble cadmium selenide nanoparticles. *J. Cryst. Growth* **2008**, *310*, 3230–3234. [[CrossRef](#)]
35. Sakellari, G.I.; Hondow, N.; Gardiner, P.H.E. Factors Influencing the Surface Functionalization of Citrate Stabilized Gold Nanoparticles with Cysteamine, 3-Mercaptopropionic Acid or L-Selenocystine for Sensor Applications. *Chemosensors* **2020**, *8*, 80. [[CrossRef](#)]